Journal of the Korean Society of Marine Engineers, Vol.28, No.8, pp.1211~1224, 2004. 11 (ISSN 1226-9549)

Measurements of a Round Jet with High-Definition 3D-PTV

Tae-Gyu Hwang† · Deog-Hee Doh* · Saga Tetsuo** · Kenneth D. Kihm***

(Manuscript : Received OCT. 21, 2004 ; Revised NOV. 3, 2004)

Abstract : Two round jets, impinged and pulsed, were measured with high-resolution 3D-PTV technique. The measurement system consists of three CCD cameras, Ar-ion laser, an image grabber and a host computer. Two fitness functions were introduced in a genetic algorithm in order to enhance the correspondences of the particles. One was based on a concept of the continuum theory and the other one was based on a minimum distance error. The velocity profiles of the impinged jet obtained by the constructed 3D-PTV system were compared with those of LDV measurements made in this study. The head vortex of the jet was visualized by LIF and was reconstructed by the constructed high-resolution 3D-PTV system for comparisons.

Key words : Impinged Jet, Pulsed Jet, Genetic Algorithm(GA), 3D-PTV, LDV, LIF

1. Introduction

Unsteady jets such as impinged and pulsed jets are seen in many industrial applications for their flow characteristics. No matter how important the jets are in applications, more fundamental studies on the structural investigation of the jets are in need. Impinged jet can be adopted many times for its outstanding cooling efficient of high-temperature plate. There has been interest in using impinged jets to dissipate the high heat fluxes found in electronic equipment such as VLSI circuits[1][2].

Olsson and Turkdongan investigated experimentally the radial flow field of an impinging liquid jet with pointwise measurement results[3]. Nakoryakov et al. discussed the flow field of an impinging jet in an experimental and theoretical study on the mass transfer and friction factor under such a jet[4]. Gardon and Akfrat discovered how the turbulent flow can effect heat transfer when free jet was impinged on the surface of a plate[5]. Kataoka et al[6]. discovered through pointwise measurements that period of

† Corresponding Author(Mechanical Engineering, Graduated School of Korea Maritime University) E-mail : andrew@bada.hhu.ac.kr
* Division of Mechanical and Information Eng., Korea Maritime University
** Institute of Industrial Science, University of Tokyo
*** Mechanical, Aerospace and Biomedical Engineering, University of Tennessee, Knoxville

vortex was dependant on the rate of heat transfer at the impinging plate. Stevens and Webb investigated the effect of nozzle configuration with the results of LDV experiments[7]. Bremhorst and Harch carried out measurements with hot-wires on the fully pulsed round air jets showed significant increases in entertainment over steady jets of the same mass flow rate. Bremhorst and Hollis measured Reynolds shear stress revealing an increase for the pulsed case but when normalized on jet momentum, levels were similar to those of the steady jet[8]. Graham and Bremhorst showed that the standard k-å model even with pulsed round jet modifications could not predict the change in slope of velocity decay correctly[9]. Nordsveen and Bremhorst found that a shear stress based model gives more accurate prediction of the propagation of the pulse but does not predict the change in velocity decay as the jet goes from pulse domination to its far field behavior of a steady jet[10]. Most of the results on the impinged and pulsed jets obtained by previous researches were based on a pointwise measurement technique such as, Hot wire and LDV, or numerical simulations. No matter how the numerical results are accurate, the results should be proved with the results obtained through an experiment because the flow fields are too complicate to be analyzed accurately. In order to attain accurate analysis on the impinged jet, it is necessary to know vortical structures of the jet. There have been some efforts to study the influence of the flow structures of an impinged jet on heat transfer. Faggiani and Grassi studied the influences of the local and average heat transfer characteristics by studying the influence of flow structure on transport as their main focuses[11] [12]. However, they showed their results on large-scaled flow structures. Hwang investigated the influences of the arrangement of an impinging jet[13]. Lee et al. investigated heat transfer characteristics at the nozzle exit configuration of turbulence axisymmetric impinging jet[14]. Bae et al. investigated the influence of the impinging angles with PIV. They could get their results with a fieldwise measurement, PIV(Particle Image Velocimetry) and LCM(Liquid Crystal Method)[15]. However, the results proposed by them were based on 2-dimensional PIV technique or 2-dimensional-field measurement technique. Borée et al. made an image analysis on a pulsed jet and indicated that at least for the production of longitudinal velocity fluctuations in a rapidly decelerating round jet, a brief period exists during which production becomes negative[16].

To make a complete analysis on the influences of the flow structures of the jets, it is even more necessary to investigate the flows 3-dimensionally as the structures have strong 3-dimensionality. None of the previous studies reports on the influences of the flow structures with the results that contain 3-dimensional properties in space except some studies reported through numerical simulations. This means that a measurement technique that can measure instantaneous vortical structures of the

jets with high resolutions is necessary in order to attain more accurate study into the influences of the vortical structures of the impinging jet on the heat transfer of heated plates.

This study focuses on an investigation into flow properties of the impinged jet and the pulsed jet with a 3D-PTV (3-Dimensional Particle Tracking Velocimetry). In Particle Tracking Velocimetry (PTV)[17], there have been many attempts to increase the number of instantaneous 3-dimensional vectors[18] [19] [20].

In the mean while, Yamada[21] and Ohyama et al[22]. adopted the genetic algorithm[23] to PTV in order to increase the number of obtained vectors. They defined a fitness function in which the displacements of every particles pair were assumed to be minimum value. They applied their GA-PTV algorithms to the measurement of a forced vortex flow field and obtained about 80% of correct vectors from initial velocity vectors. Doh et al. gained more than 98% of correct vectors from initial velocity vectors for the same flow field with virtual images[24]. They took a consideration into the disappearing particles pairs between two image frames. Their idea was to preserve a recessive group of the particles that were generally thrown away in the calculation process of genetic algorithm. Most of the conventional PTVs or GA-PTVs were mainly concerned with two-dimensional measurements.

In this study, a new High-Vision 3D-PTV system was constructed by adopting a new GA-PTV algorithm for the study of an impinged jet and a pulsed one. The measurement system could obtain more than 5,000 instantaneous three-dimensional velocity vectors for an impinging jet with three high-resolution cameras (1016 x 1000 pixels). Several quantitative results on the jets have successfully been obtained by the constructed system. It was verified that the constructed 3D-PTV system would be able to be compatible with the results of DNS if high-resolution cameras are systematically installed with the system.

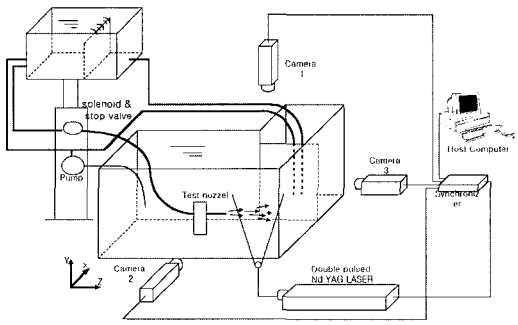

Fig. 1 High-definition 3D-PTV system for the jet experiments.

2. Measurement of Jets

2.1 Experimental setup and procedure

Fig. 1 shows the overall arrangement for the measurements of the impinged jet and the pulsed jet. The diameters (d) of the nozzles for two experiments are 3.0mm and 3.4mm, respectively. The measurement system consists of three cameras (Kodak ES1.0, 1,000 x 1,016 pixels), an image grabber (TSI) in the host computer(Pentium III) and a Nd-YAG laser. The three cameras were synchronized with a synchronizer. The jet

was installed in a water tank (800 x 600 x 400mm). A plate (100 x 100mm) was installed in front of the nozzle with a distance of 10d. Reynolds number (UD/ν) was about 3,000. ν is the kinematic viscosity at 20℃. The origin of the absolute coordinate (X=0, Y=0, Z=0) for the impinged jet was defined at the center position between the nozzle and the plate along the centerline of the jet. The origin for the pulsed jet was set at the nozzle tip. The measurement volume for the impinged jet is (X:30mm, Y:30mm, Z:30mm) and for the pulsed jet is (X:20mm, Y:20mm, Z:20mm). A traverse was used as mentioned for camera calibration and was moved in the volume with 4mm and 6mm steps for each experiment for the impinged jet and for the pulsed jet. On the tip of the traverse, a ball (diameter: 2mm, accuracy: 20μm) was installed. This ball was moved three-dimensionally with the traversing steps as shown in Fig. 2. In order to produce a pulsed jet, a solenoid valve was installed ahead of the exit of the nozzle. The position of the location is the same place where the stop valve located for the impinged jet experiment. The opening time of the solenoid valve was synchronized with the signal of the PTV system. The duration of the valve opening was 500μsec. After completing the calibration for the three cameras and the construction of the flow field, tracers (Glass Hollow-AG) were seeded into the circulating water channel and a Nd-YAG laser (200mJ) located at a position where the light was backscattering for the three cameras was illuminated. The illuminating time of the laser light is synchronized with the whole camera system.

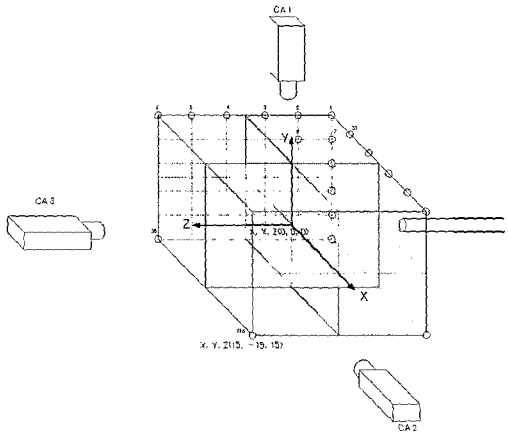

Fig. 2 Calibration landmarks.

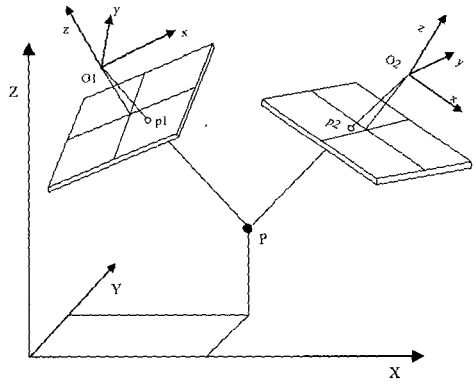

Fig. 3 Relations between the absolute and the photographic coordinate definition of 3D positions of particles.

2.2 High-definition 3D-PTV system

In order to construct a high-definition(resolution) 3D-PTV system, high-resolution cameras and an image grabber were constructed with 3D-PTV algorithm. To get the three-dimensional velocity vectors, exterior parameters of camera such as, the position and the

orientations of the camera, interior parameters representing the focal length, deviations of the principal point and the distortion coefficients of the camera lens was obtained in advance. Next, three-dimensional position of each particle was calculated. Finally, three-dimensional velocity vectors were calculated. For camera calibration, the traverse was moved in stepwise to the landmarks positions as shown in Fig. 2 where calibration images were pictured. Some processing such as noise reduction and thresholding were carried out on the images to get more accurate photographic coordinates of landmarks.

Nishino[25] and Doh et al[26]. used 11 parameters that crucially decide the cameras orientation. However, the whole processes obtaining the parameters were so complicated. In this study, 10 parameter methods (6 exterior parameters: $dis, \alpha, \beta, \varkappa, m_x, m_y$, 4 interior parameters: c_x, c_y, k_1, k_2) proposed by Doh et al. was introduced to improve the camera calibration[24] [27].

Here, *dis* means the distance between the origin O(0, 0, 0) and the principle point (X_0, Y_0, Z_0) of the camera on the absolute coordinate. ($\alpha, \beta, \varkappa$) is the tilting angle of the axis of the camera coordinate (photographical coordinate) against the axis of the absolute. The m_x, m_y mean the point at which the normal vector from the origin O(0, 0, 0) of the camera coordinate and the X-Y plane of the absolute coordinate meet. c_x and c_y are the focal distances for each component of the coordinate. k_1 and k_2 imply lens distortion factors.

The three-dimensional position of a particle could be obtained as an intersection of corresponding perspective rays from the two cameras as shown in Fig. 2. The collinear equation for each camera was given as Eq. 1.

$$\begin{pmatrix} X \\ Y \\ Z \end{pmatrix} = \begin{pmatrix} a_{11} & a_{12} & a_{13} \\ a_{21} & a_{22} & a_{23} \\ a_{31} & a_{32} & a_{33} \end{pmatrix} \begin{pmatrix} x \\ y \\ -c \end{pmatrix} + \begin{pmatrix} X - X_o \\ Y - Y_o \\ Z - Z_o \end{pmatrix} \tag{1}$$

Here, X, Y and Z are the absolute coordinates transformed from the image coordinates, x and y. c is composed of c_x and c_y. The elements of the rotation matrix a_{ij} were obtained from the camera calibration. Three cameras (A, B, C) were used to get three-dimensional vectors in this study and each two-camera set, (A, B) and (A, C), was contributed to produce the last three-dimensional velocity vectors. Mathematically speaking, since the corresponding perspective rays of the two cameras do not intersect due to unavoidable uncertainties associated not only with the cameras parameters but also with the particles' centroids, a calculation process in which decision of the coordinate (X, Y, Z) in Eq. (1) was adopted using the least square method. The three-dimensional positions of every particle using the two cameras (A, B) were defined as the following Eq. (2).

$$\begin{bmatrix} X_P \\ Y_P \\ Z_P \end{bmatrix} = \frac{1}{2} \left\{ \begin{bmatrix} X_A \\ Y_A \\ Z_A \end{bmatrix} + \begin{bmatrix} X_B \\ Y_B \\ Z_B \end{bmatrix} \right\} \tag{2}$$

Here, X_A, Y_A and Z_A were defined as the coordinate components that were decided by the use of Eq. (1) for camera A. X_B, Y_B and Z_B were also defined for

camera B. In order to calculate the three-dimensional positions of particles, corresponding pairs the centroids of particles of the two camera images should be discovered among many other particles. A genetic algorithm was used to find the corresponding pairs. Here, genetic algorithm has been adopted in order to make the true pairs remain until the whole possible pairs between the two sets of cameras, (A, C) or (A, C), are determined simultaneously. Table 1 shows the definition of chromosome used in PTV for particles pairing. Detailed calculation procedure is well explained in the reference[27]. Four major GA operators, isolation, reproduction, crossover and migration were introduced. A chromosome consists of two coordinates of both cameras. The initial population was generated through a calculation process in which a threshold value was introduced to discriminate the worst particle pairs that had large *3DE* values expressed in Eq. (3).

$$D=\sqrt{(X_B-X_A)^2+(Y_B-Y_A)^2+(Z_B-Z_A)^2} \tag{3}$$

where, $3DE = 1/2(D_s + D_e)$

Ds: 3-dimensional positional error between the origin of two vectors

De: 3-dimensional positional error between the terminal of two vectors

Camera 1		Camera 2		fitness function	
Start point	End point	Start point	End point	3DE	Conti -uity
coordi-nate of particle (x_{11}, y_{11})	coordi-nate of particle (x_{12},y_{12})	coordi-nate of particle (x_{21},y_{21})	coordi-nate of particle (x_{22}, y_{22})	Eq.(3)	Eq.(4)

$$C=\left|\frac{\partial u}{\partial x}\right|_{\min}+\left|\frac{\partial v}{\partial y}\right|_{\min}+\left|\frac{\partial w}{\partial z}\right|_{\min} \tag{4}$$

Eq. (3) implies that the distance between the two collinears viewed by the two cameras has the minimum value. After the initial population was decided, an isolation process was operated using the same *3DE* value. The particle pairs having a value larger than a threshold *3DE* value were isolated to the unselected group. Next, a reproduction process was made. In the reproduction process, a fitness function as expressed as Eq. (4) based on a continuity concept was used for a refinement of the selected group[27]. Finishing the reproduction process, a crossover process was adopted. In this process, the photographical data of the two- dimensional vectors of each camera were exchanged and an elimination process was made referencing the *3DE* value again. In order to give a revival chance to the particles sorted into the inferior group up to now, a migration process was adopted. This process is similar to the initialization process. The above processes are repeated up to 10-15 generations. The threshold value *3DE* is 0.5mm and the crossover portion is 15% among the whole chromosomes generated. During the calculation of GA, operators such as, isolation, reproduction, crossover and migration (this concept belongs to mutation) were recursively used until the last optimized solution of the two objective fitness functions with Eq. (5) and the one based on a continuity concept were found, whch implies the pairs of particles were decided. The three-dimensional velocity vectors were

then obtained by dividing the distances between the last paired particles by the time interval Δt.

2.3 Experimental results on impinged jet

Fig. 4 shows one of grabbed images of the flow pictured by camera 2. Each particle occupies 2-9 pixels on average. Since the pixels of one particle was not so enough to calculate the centroids of the particles, a masking method was used[28]. Fig. 5 shows instantaneous raw velocity vectors obtained by the constructed system. The number of instantaneous 3D vectors obtained was about 6000 with spurious vectors. Spurious vectors were eliminated before the interpolation using Tomsons value[25]. The number of vectors regarded as correct ones was about 4000 to 5200. The velocity vectors obtained within the measurement region. The raw vectors were interpolated onto the grids of 16 x 16 x 16 using a Gaussian window[29]. Fig. 6 shows the interpolated instantaneous three-dimensional vectors on the grids.

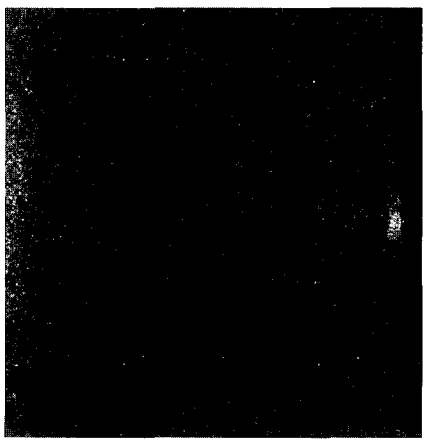

Fig. 4 Raw images captured by camera 2.

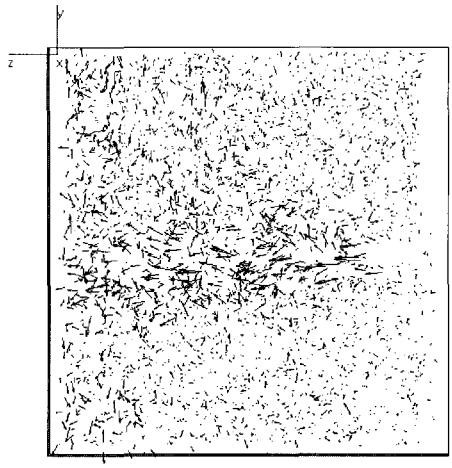

Fig. 5 Obtained instantaneous 3D velocity vectors.

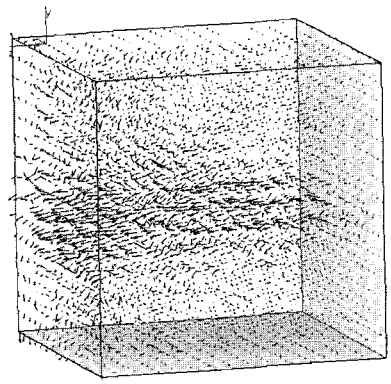

Fig. 6 Instantaneous 3D vectors on grids.

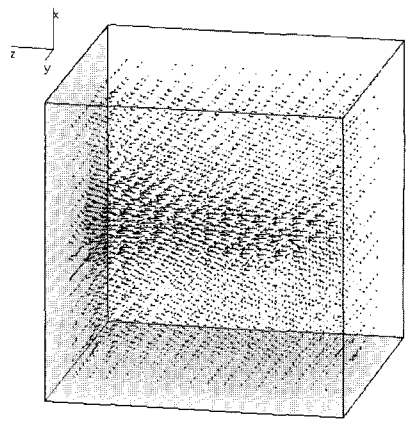

Fig. 7 Time-mean 3D velocity field on grids (16 x 16 x 16).

Fig. 7 shows a time-mean 3D velocity field. And Fig. 8 shows the velocity profiles. The black lines mean the results obtained through a LDV measurement.

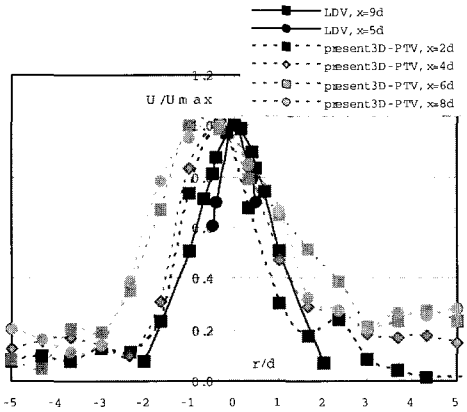

Fig. 8 Velocity profiles (LDV, 3D-PTV).

The dotted lines with several shapes such as square and circle show the results obtained by the constructed 3D-PTV. There are some discrepancies between the results of LDV and those obtained by the 3D-PTV. However, the velocity profiles are very similar each other. It is estimated that the discrepancies were due to the discrepancy of the nozzle directions when the two experiments, LDV and 3D-PTV were carried out. As another factor for the discrepancies seems to be due to the blocking effect of the particles to the nozzle when 3D-PTV experiments was carried out. In case of LDV experiments, the blocking effect is negligible since Rhodamin B ink has been used as tracers. Some conspicuous results can be summarized from the results obtained by the constructed 3D-PTV system. There is some similarity in the velocity profiles within the region where the radius is less than r/d=4.0 at upstream region. But, this similarity disappears at downstream. Further, there is no similarity in the region where the radius is larger even if the region is upstream. In the meantime, there seems also another similarity near the flat plate that was installed for the impingement of the jet in the region where the radius is larger than r/d=3.0.

Fig. 9 Instantaneous vorticity distribution (I-component) (Red = positive, Blue= negative)

Fig. 9 shows an instantaneous vorticity distribution of I-component. The result shows only one value of vorticity contour. Red colored means positive and and blue one means negative. From this figure, it can be said that there exists minus and plus signed vorticities at an instance among many vorticity values. This quantity will not be able to be captured with other measurement methods. It can be said that the constructed High-Vision 3D-PTV system could probe instantaneous vortical structures of the impinged jet flow.

2.4 Testimonial experiment on a pulsed jet with LIF visualization

The constructed system can capture instantaneous flow structures since it can obtain more than 5,000 instantaneous three-dimensional vectors. This means that the system not only makes possible to obtain the temporal evolution of turbulence properties but also makes possible to capture the instantaneous flow structures. Further, this implies the possibility of unveiling the energy budget of turbulences. Unfortunately, there has been no experimental report that provides the energy budget of turbulent properties, quantitatively. Pulsed jet is the best flow field in investigating the energy budget. Accordingly, a pulsed jet experiment was carried out as a test experiment to verify the performance of the constructed 3D-PTV system in providing quantitative energy budget of turbulences.

LIF(Laser Induced Fluorescence) visualization was carried out to compare qualitatively the results obtained by the constructed 3D-PTV system, which will eventually ensure that the constructed 3D-PTV system can be used in any unsteady flow fields. The jet is pulsed only once by opening a solenoid valve and closing it. The solenoid valve was synchronized with the signal of the PTV system through a signal controller (LabSmith LC880) and the opening time of the solenoid valve was 1 sec after activating the laser system. The duration of the valve opening was 500μsec.

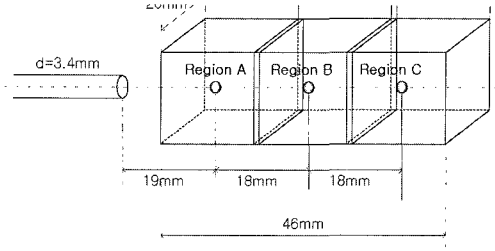

Fig. 10 Measurement region with High-Definition 3D-PTV system

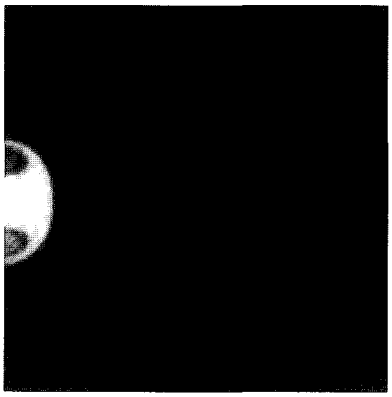

(a) LIF image

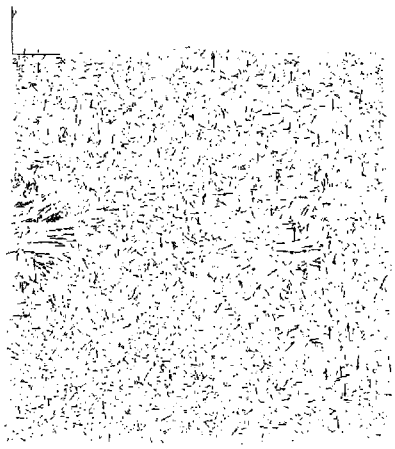

(b) 3D-PTV results

Fig. 11 Results at the time of t = to.

The measurement system is the same as the setup for the experiments for the impinged jet except a solenoid valve is

installed for generating a pulsed jet. A traverse was used as mentioned for camera calibration and was moved in the volume with 4mm step. Measurement volume is configured in Fig. 10. Three regions were setup. However, the visualization results obtained by LIF and by the 3D-PTV are presented only in the region A in this study. Three camera were installed toward the region A. The traverse that has a small ball at its tip was moved in the region A in stepwise and the images of the ball were captured by the three cameras. After completing camera calibration, main experiment was carried out with the same measurement algorithm. The number of instantaneous 3D vectors obtained by the constructed 3D-PTV system was ranging from 4,000 to 6,000 in this experiment.

Fig. 11 and Fig. 12, show the sequential results obtained by LIF and the constructed 3D-PTV system. The time interval of each result is 0.1 sec (1/10Hz). All time sequences and timing of the two systems are same. Figures (a) and (b) show the LIF images and the instantaneous three-dimensional vector distribution obtained by the constructed 3D-PTV system. From these figures, it can be said that the structures of the LIF images at every instance are quite similar to the distribution of instantaneous three-dimensional vectors. These results do not assure that the constructed 3D-PTV system can completely capture the instantaneous flow structure. However, the results obtained by the constructed 3D-PTV system show quite reasonable structures qualitatively when compared with the LIF images though they are not quantitative ones. Quantitative analysis on the pulsed jet will be reported in the next manuscripts.

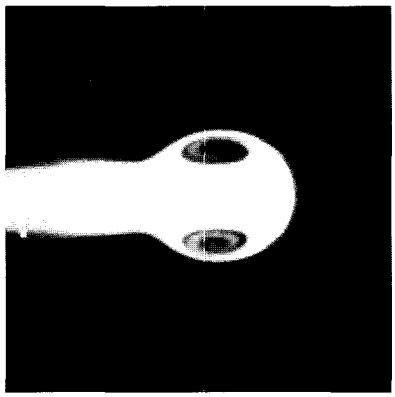

(a) LIF image

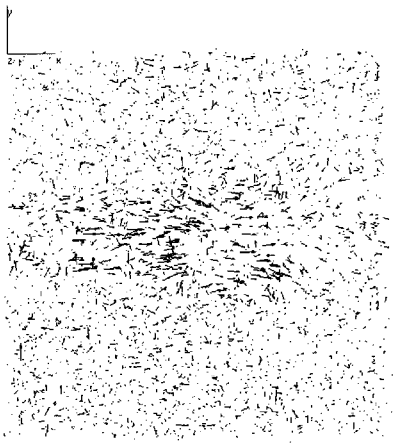

(b) 3D-PTV results

Fig. 12 Results at the time of t = to + 1/10 sec.

3. Conclusions

A new High-Resolution 3D-PTV technique was constructed through an experiment on an impinged jet using non-metric high-vision three digital cameras and a genetic algorithm (GA).

The constructed system can capture instantaneous flow structures since it can obtain more than about 5,000 to 10,000 instantaneous three-dimensional vectors. This number is the highest among other three-dimensional PTV techniques up to now, which also implies the possibility of direct probing of flows if more high-definition cameras and video systems are adopted.

The properties of the impinged jet obtained by the constructed High-Resolution 3D-PTV system showed qualitatively reasonable comparing with those obtained by LDV measurements made in this study.

It seemed that there is a similarity law in the regions of the impinged jet where the radius r/d is less than 4.0 at upstream and where the radius is larger than 3.0 near the flat plate.

The results obtained in the experiment of the impinged jet implies that the system not only makes possible to obtain the temporal evolution of turbulence properties but also makes possible to capture the instantaneous flow structures. Further, this implies the possibility of unveiling the energy budget of turbulences.

Since the pulsed jet is the best flow field in investigating the energy budget of turbulences, a test measurement with LIF visualization was carried out with the constructed 3D-PTV system.

Quantitative analysis on the pulsed jet will be reported in the next manuscripts.

The constructed system will be able to be used for the investigation of the turbulent properties of complex flows such as wakes, jets and other complex flows.

This work was supported by Korea Research Foundation Grant KRF-2004-002-D00082 and partly by BK21 and IIS of Tokyo Univ.

References

[1] Kiper, A.M., 1984, "Impinging water jet cooling of VLSI circuits", International Communications in Heat and Mass Transfer, Vol.11, pp.517-526.

[2] Yamamoto, H., Udagawa, Y., Suzuki, M., 1987, "Cooling System for FACOM M-780 Large-Scale Computer", Proceedings of the International Symposium on Cooling Technology for Electronic Equipment, pp.96-109.

[3] Olsson, R.G., Turkdogan, E.T., 1966, "Radial spread of a liquid stream on a horizontal plate", Nature, Vol.211, pp.813-816.

[4] Nakoryakov, V.E., Pokusaev, B.G., Troyan, E.N., 1978, "Impingement of an axisymmetic liquid jet on a barrier", International Journal of Heat and Mass Transfer, Vol.21, pp.1175-1184.

[5] Gardon, R., Akfrat, J.C., 1965, "The role of turbulence in determining the transfer characteristics of impinging jet", Int. J. Heat Mass Transfer, Vol. 8 pp.1261-1272.

[6] Kataoka, K., Mihata, I., Maruo, K., Suguro, M., Chigusa, T., 1986, "Quasi periodic large scale structure responsible for the selective

enhancement of impinging jet heat transfer", Proceeding of the 8th Int. Heat Transfer Conf. Vol. 3, pp.1193-1198.

[7] Stevens, J., 1992, "Measurements of local fluid velocities in an axisymmetric. Free liquid jet impinging on a flat flate", Ph.D. Dissertation. Brigham Young University, Provo. UT.

[8] Bremhorst, K., Hollis, P. G., 1990, "Velocity field in an axisymmetric pulsed subsonic air jet", AIAA J., Vol.28, No.12, pp.2043-2049.

[9] Graham, L. J. W., Bremhorst, K, 1993, "Application of the k-å turbulence model to the simulation of a fully pulsed free air jet", ASME, J. Fluids Eng., Vol.115, No.71, pp.70-74.

[10] Nordsveen, M., Bremhorst, K., 1998, "Simulations of a fully pulsed round turbulent air jet flow with k-å and Reynolds stress turbulence models", Proc. of 13th Australasian Fluid Mechanics Conf., Monash Univ., Melbourne, Australia, pp.95-98.

[11] Faggiani, S., Grassi, W., 1990a, "Impinging Liquid Jets on Heated Surfaces", Proceedings of the Ninth International Heat Transfer Conference, Vol. 1, pp.275-285.

[12] Faggiani, S., Grassi, W., 1990b, "Round Liquid Jet Impingement Heat Transfer: Local Nusselt Numbers in the Region With Non Zero Pressure Gradient", Proceedings of the Ninth International Heat Transfer Conference, Vol. 4, pp. 197-202.

[13] Hwang, S.D., Lee, C.H., Cho, H.H., 1999, "An Experimental study on flow and heat transfer characteristics of circular impinging jet with acoustic excitation", Proceeding of KSME thermal engineering. pp.122-129.

[14] Lee, J.H., Lee, S.J., 1999, "Heat transfer enhancement based on nozzle exit configuration of turbulent axisymmetric impinging jet, Proceeding of KSME thermal engineering", pp.122-129.

[15] Bae, S. T., Kim, D. K., Kim, S. B., "An experimental study on flow characteristics of impinging jet", Journal of the Korean Society of Marine Engineers, Vol. 25, No.2. pp.173-179.

[16] Borée, J., Atassi, N., Charnay, G., Taubert, L., 1997, "Measurements and image analysis of the turbulent field in axisymmeric jet subject to a sudden velocity decrease", Exp. Thermal and Fluid Sci, Vol. 14, pp.45-51.

[17] Adrian, R.J., 1991, "Particle-imaging techniques for experimental fluid mechanics", Ann. Rev. Fluid Mech. Vol.23, pp.261-304.

[18] Kasagi, N., Nishino, K., 1991, "Probing turbulence with three dimensional particle tracking velocimetry", Exp. Thermal and Fluid Sci. Vol.4, pp.601-612.

[19] Mass, H.G., Gruen, A., Papantoniou, D.A., 1993, "Particle tracking velocimetry in three-dimensional flows, Part 1 Photogrammetric determination of particle coordinates", Exp. in Fluids, Vol.15, pp.133-146.

[20] Doh, D.H., Kim, D.H., Choi, S.H., Hong, S.D., Saga, T., Kobayashi, T.,

2000a, "Single-Frame (Two-Field Image) 3D-PTV for high speed flows", Exp. in Fluid, Suppl., pp.85-98.

[21] Yamada, H., Yamane, K., 1995, "Particle Image Velocimetry using a genetic algorithm", J. of Flow Visualization Soc. Jpn., Vol.15, Suppl. No.1, pp.165-168.

[22] Ohyama, R., Takagi, T., Tsukiji, T., Nakanishi, S., Kaneko, K., 1993, "Particle tracking technique and velocity measurement of visualized flow fields by means of genetic algorithms", J. of Flow Visualization Soc. Jpn., Vol.13 Suppl. No.1, pp.22-25.

[23] Goldberg, D.E., 1985, "Optimal initial population size for binary-coded genetic algorithm", TCGA Report No. 85001. University of Alabama.

[24] Doh, D.H., Kim, D.H., Cho, K.R., Cho, Y.B., Saga, T., Kobayashi, T., 2001, "3D-PTV using Genetic Algorithm", Proc. CD-ROM of 4th International Symposium on PIV, Gottingen, Sep. 17-19, 2001, Paper No.A1050.

[25] Nishino, K., Kasagi, N., Hirata, M., 1989, "Three-dimensional particle tracking velocimetry based on automated digital image processing", ASME J. Fluids Eng., Vol.111, No.4, pp.384-391.

[26] Doh, D.H., Cho, K.R., Baek, T.S., Cho, Y.B., 2000b, "3D-PTV using a Genetic Algorithm", Proc. of Winter Annual Conference, the Society of Air-conditioning and Refrigeration Engineers of Korea, Korea, Vol.2, pp.601-605.

[27] Doh, D. H., Kim, D. H., Cho, K. R., Cho, Y. B., Lee, W. J., Saga, T., Kobayashi, T., 2002, "Development of Genetic Algorithm based 3D-PTV technique, Journal of Visualization", Vol.5, No. 3 pp. 243-254.

[28] Takehara, K., Etoh, T., 1999, "A study on particle identification in PTV Particle Mask Correlation Method", Journal of Visualization, Vol.1 No.3, pp.313-323.

[29] Agui, J.C., Jimenez, J., 1987, "On the performance of particle tracking", J. Fluid Mech., Vol. 185, pp.447-468.

Author Profile

Tae-Gyu Hwang

He received a B.A at Korea Maritime University in 2001. He finished his M.Sc. degree at Korea Maritime University (KMU) in 2003. He is a Ph.D candidate of mechanical engineering at KMU since 2003. His recent research area is on the near wake of a sphere using 3D PTV and on an impinged jet flow using 4D-PTV technique. His research interests are thermal flow visualization using 3D-PIV, 3D-PTV and micro PIV techniques.

Deog-Hee Doh

He received a B.A. at Korea Maritime University (1985). He finished his M.Sc. degree at the graduate school of Korea Maritime University (1988). He received his PhD. degree at the Department of Mechanical Engineering of the University of Tokyo, Japan in 1995. His graduate works is issuing the development of 3D-PTV and simultaneous measurement techniques on temperature and velocity fields for thermal turbulent flows. He worked as an invited researcher for the Advanced Fluid Engineering Research Center (AFERC) in 1995. He has been working for Korea Maritime University since 1995 at the School of Mechanical and Information Engineering. His major research subjects are to develop spatial measurement techniques such as 3D-PIVs, 3D-PTVs for the analysis of turbulent flows.

Saga Tetsuo

He graduated from Japan University in 1966 and he is a research associate in the Institute of Industrial Science, the University of Tokyo. His main research field is mechanical engineering. His research interests include flow visualization and its image analysis, prediction and control of flow induced vibration and automobile aerodynamics. Recently, he has interests in micro flow and bio flow analysis using PIV.

Kenneth D. Kihm

He received his doctoral degree in Mechanical Engineering from Stanford University in 1987, successively after he received his BS (1979) and MS (1981)-degree from Seoul National University in Korea. During his career with Texas A&M University since 1988, Dr. Kihm initiated and established an interdisciplinary research field in thermal transport and fluidic phenomena in micro/nano-scale for the Department of Mechanical Engineering. He is currently holding the Magnavox Chair Professorship at Mechanical, Aerospace and Biomedical Engineering of University of Tennessee in Knoxville. He also serves as the director of Micro/Nano-Scale Fluidics and Energy Transport (MINSFET) Laboratory (http://www.engr.utk.edu/~minsfet).

His research interest is in development and applications of advanced optical diagnostic techniques for micro/nano/bio-fluidics and heat transfer problems.